Results in Optics 13 (2023) 100531

Contents lists available at ScienceDirect

Results in Optics

journal homepage: www.sciencedirect.com/journal/results-in-optics

Optical and structural investigation of methylammonium lead perovskite mixed halide (I, Br, and Cl) on spin-coated zinc oxide

Klègayéré Emmanuel Koné [a,*], Amal Bouich [a,c,*], Bernabé Marí Soucase [a], Donafologo Soro [b]

[a] Departament de Física Applicada, Instituto de diseño y Fabricació (IDF), Universitat Politècnica de València (UPV), Cami vera, Spain
[b] Département des Sciences et Technologie, Ecole Normale supérieure (ENS) d'Abidjan, Cocody, Côte d'ivoire
[c] Física Applicada a las Ingeniereas aeronáutica Naval & Instituto de Energía Solar, Universidat politécnica de Madrid, Spain

ARTICLE INFO

Keywords:
Perovskite
Mixing
ZnO
Heterojunction
Thin film
Stability

ABSTRACT

This study investigated the effect of mixing different halides bromine (Br) with iodine (I) and Br with chlorine (Cl) and using only bromide for methylammonium lead perovskites films deposited in ZnO to produce different heterojunctions ZnO/MAPbBr$_3$, ZnO/MAPbBr$_2$I and ZnO/MAPbBr$_2$Cl. Thus, these three heterojunction samples were produced and characterized. The perovskite is deposited at ZnO films showed two main peaks located at $2\theta = 33.66^\circ$ and $2\theta = 37.69^\circ$. These peaks correspond to the (002) and (101) planes of the hexagonal wurtzite structure of ZnO respectively. The XRD results indicate that all the heterojunction samples show two main peaks at $2\theta = 14.79^\circ$ and $2\theta = 29.83^\circ$ for the (100) and (200) crystallographic planes respectively. The peaks of the sample mixed with iodine are the most intense and those of the sample mixed with chlorine are the least intense. These results also reveal that the mixed samples have lower crystallinity than the unmixed ZnO/MAPbBr$_3$ sample. The SEM results confirmed this. The UV–Visible results indicate that the sample mixed with iodine absorbs the most and has the smallest band gap of 2.15 eV. The band gaps of the heterojunctions range from 2.15 eV to 2.4 eV. The unmixed sample (ZnO/MAPbBr$_3$) has the largest band gap. The degradation study showed that the sample mixed with iodine degrades faster.

1. Introduction

Through human activities, the world is developing year by year. This development is the result of progress in every area of life. Among these areas, photovoltaic energy is not left out. Photovoltaic cells have progressed since the first cells were made of silicon. Research has led to the discovery of other types of materials such as Copper Indium Gallium Sulfur (CIGS), CdTe, and organic cells that can be used as absorbing layers in a solar cell (Oyedele et al., 2017; Bouich et al., 2022; De Wolf et al., 2014; N'guessan et al., 2023). The discoveries continued until the discovery of perovskite, a new material with good efficiency compared to previous ones (Touré et al., 2023; Bouich et al., 2023). A perovskite generally consists of three groups of molecules or atoms which are in the form ABX_3 (A = Cation (Formamidinium (MA^+)), Methylammonium (FA^+), Cs^+; B = metal cation (Pb_2^+, Sn_2^+) and X = halogen anio (Br^-, Cl^-, I^-)) (Bouazizi et al., 2022; Bouri et al., 2022). This absorbing perovskite layer has interesting optical properties. It has good light absorption in the UV–visible (De Wolf et al., 2014), an interesting diffusion length (Stranks et al., 2013; Xing et al., 2013), a good charge carrier conductivity (Leijtens et al., 2015; Leijtens et al., 2014), a higher photovoltaic conversion efficiency (PCE) (Fakharuddin et al., 2019; Weidman et al., 2019; Bouich et al., 2023). The absorber layer of a solar cell is usually deposited on an electron transport layer (ETL) which can be zinc oxide (ZnO). Zinc oxide layer is a protective layer and protects the absorbent layer against corrosion (Gledhill et al., 2009). It has piezoelectric and optical properties that allow it to be used as an ETL and it is also used in gas detection (Hwang et al., 2009). ZnO also has great potential for photocatalytic (PC) applications in environmental treatments, such as wastewater degradation, drinking water sterilization, and air purification (Gu et al., 2016). Perovskite-based solar cells have developed very rapidly because they have a great advantage in the field of solar energy (Burschka et al., 2013; Im et al., 2011; Jeon et al., 2015; Kojima et al., 2009; Lee et al., 2012). The power conversion efficiency (PCE) of these cell types has skyrocketed to a record 22% (Zhou et al., 2014), which is close to the best value of polycrystalline silicon cells (Masuko et al., 2014). The excellent performance of perovskite solar cells is due to the high absorption coefficient, low exciton binding energy, and long diffusion length of perovskite films (Kojima et al., 2009;

* Corresponding authors.
E-mail addresses: koneemmanuel277@gmail.com (K. Emmanuel Koné), ambo1@doctor.upv.es (A. Bouich).

https://doi.org/10.1016/j.rio.2023.100531
Received 17 April 2023; Received in revised form 23 August 2023; Accepted 21 September 2023
Available online 22 September 2023

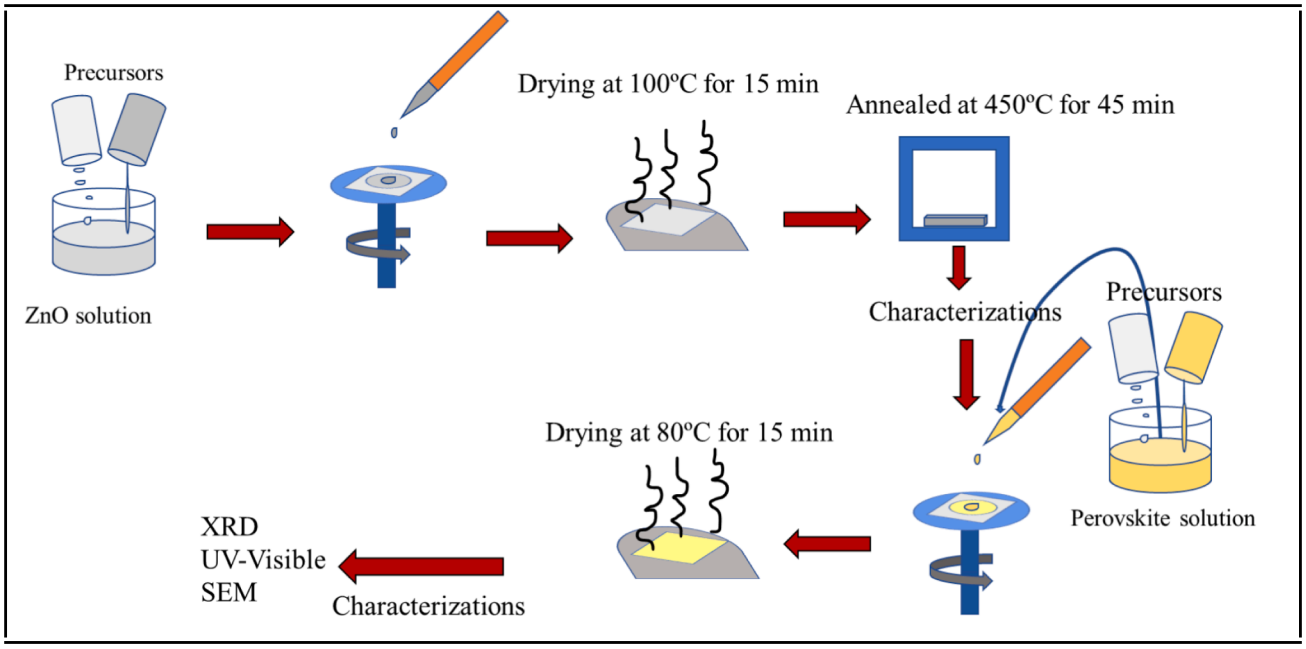

Fig. 1. Schematic of perovskite deposition on ZnO film by spin-coating.

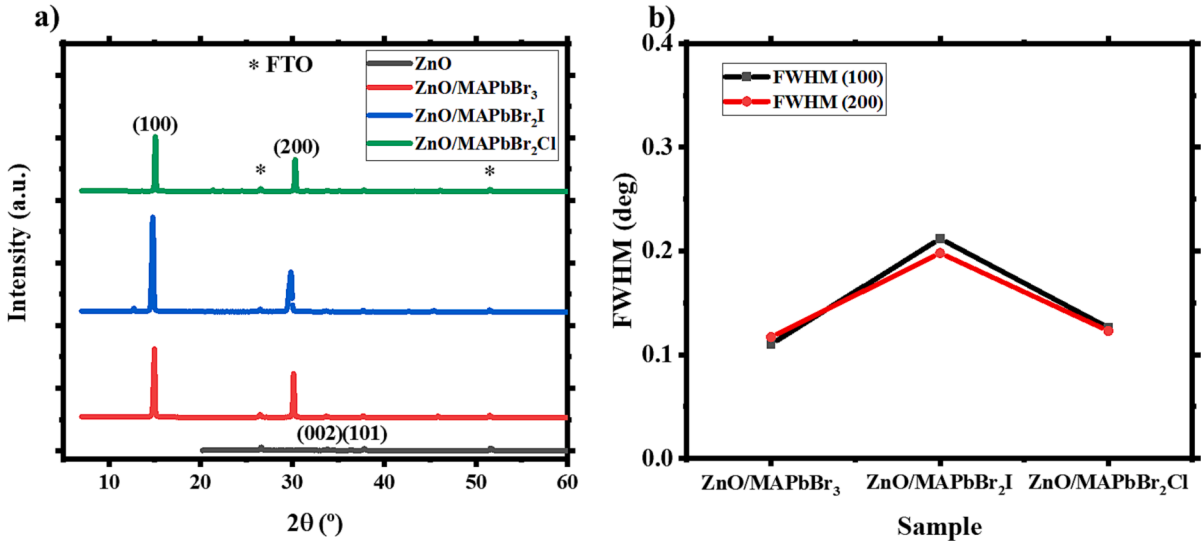

Fig. 2. A) xrd patterns of samples; b) fwhm of heterojunction samples.

Table 1
Grains size, dislocation density, and lattice strain of samples.

Samples ID	Grains size D (nm)	Dislocation density δ (nm^{-2})	Lattice strain ε
ZnO	401	6.22×10^{-6}	0.173
$ZnO/MAPbBr_3$	747	1.79×10^{-6}	0.159
$ZnO/MAPbBr_2I$	414	6.83×10^{-6}	0.350
$ZnO/MAPbBr_2Cl$	681	2.16×10^{-6}	0.176

Lin et al., 2015; Stranks et al., 2013; Zhao et al., 2015). In a solar cell, the perovskite layer is either deposited on a hole transport layer (HTL) or on an ETL, thus forming a heterojunction (Shao et al., 2020). Many semiconductor materials are potential candidates for the construction of a heterojunction with a perovskite. Among them, zinc oxide is a promising candidate because of its excellent optical and electrical properties. Indeed, it has a wide direct band gap of about 3.37 eV, a high exciton binding energy of 60 meV, high carrier mobility and good stability (Chang et al., 2006; Look et al., 2003).

The novelty of this work is not only to study the properties of the different layers of the heterojunction but also to study the interface between the layers and especially the optical and structural properties of the two layers together.

Many methods are used to produce perovskite. These include the

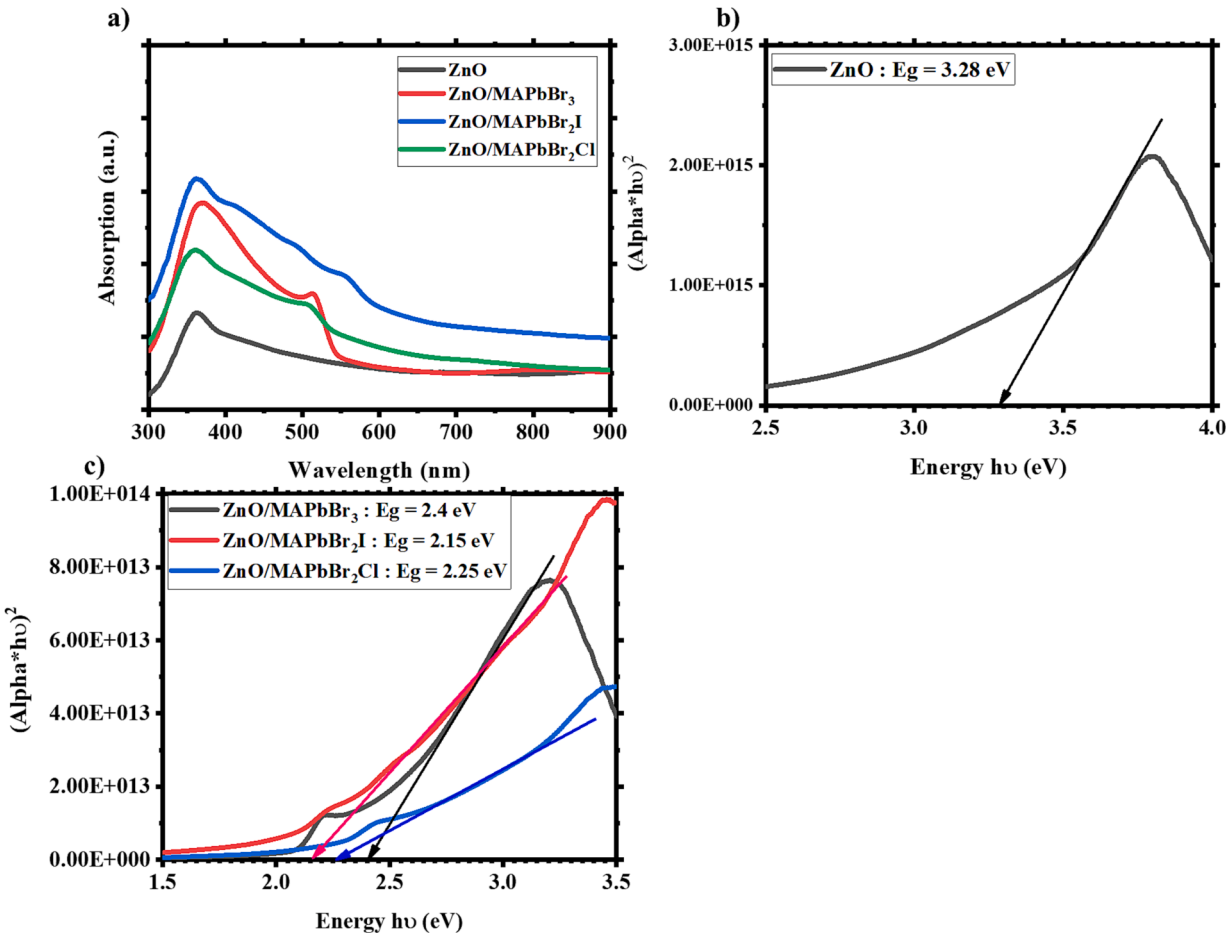

Fig. 3. Optical properties of films product: a) Absorbance of samples, b) band gap of ZnO, c) band gap of heterojunction films.

printing technique (Schmidt et al., 2015), inkjet (Zhou et al., 2014), dip-coating, and spin-coating (Tang et al., 2021). The spin-coating technique was used in this work because it is lower cost and simple.

Although perovskite is a great asset for photovoltaics, it has weaknesses, especially in the area of stability. A study has shown that $MAPbI_3$ is less stable than $MAPbBr_3$ and $MAPbCl_3$ but has more interesting properties (Koné et al., 2023). In order to improve the properties of $MAPbBr_3$ as well as its stability, we chose to mix halogens. Thus, in this work, we produced ZnO layers and characterized them. On each of these layers, a perovskite layer ($MAPbBr_3$; $MAPbBr_2I$, and $MAPbBr_2Cl$) was deposited by the spin-coating method. The different layers produced were characterized and their stability was studied.

2. Experimental procedure

The spin-coating technique was used to make the deposits on Fluorine doped Tin oxide (FTO) glass substrates. The deposits were made in two steps: first, the zinc oxide was deposited on the FTO, and after the different characterizations, the perovskite solution was deposited on the ZnO. the zinc oxide solution was prepared by dissolving dehydrated zinc acetate [$Zn(CH_3COO)_2$, $2H_2O$] > 99.5% purity in ethanol solution to obtain a 0.5 M solution. After that, the solution was placed on the FTO which was rotated at 3000 rpm for 30 s. The films obtained were annealed in an oven at 450 °C for 45 min. After characterizations, the same films were used for the deposition of perovskite. To do so, we prepared the three perovskite solutions using different precursors. The iodine-based precursors were dissolved in N, N-dimethylformamide (DMF), and the bromine-based precursors in dimethyl sulfoxide (DMSO 99.9%). The $MAPbBr_3$ solution was prepared using methylammonium bromide (MABr) and lead bromide ($PbBr_2$). The $MAPbBr_2I$ solution was prepared using methylammonium iodide (MAI) and lead bromide ($PbBr_2$) and the $MAPbBr_2Cl$ solution by dissolving methylammonium chloride (MACl) and lead bromide ($PbBr_2$).

The perovskite solutions thus prepared were each deposited on a ZnO film by the spin-coating method. A few moments after the start of the spin-coating, a few drops of ether were poured onto the spinning substrate. This will allow for obtaining good morphology and crystallinity of the films. The obtained films were annealed on the plate at 80 °C. Fig. 1 below shows the deposition procedure.

2.1. Characterizations techniques

We characterized the samples by absorption spectrometry (SPECTROVIO C521O-C5220) with an input slit. In the 400–800 nm wavelength range, 50 μm × 100 μm were recorded. Also, we used the XPERT-PRO diffractometry system, the XRD monochromator, to characterize the samples by X-ray diffraction. This system was used to perform structural characterization of the samples with a wavelength of 0.15406 nm, 20 kV, and Cu-kα radiation. The results are based on Bragg's law. Morphological images of the samples were taken by scanning electron microscopy (SEM) with an acceleration voltage of 25 kV.

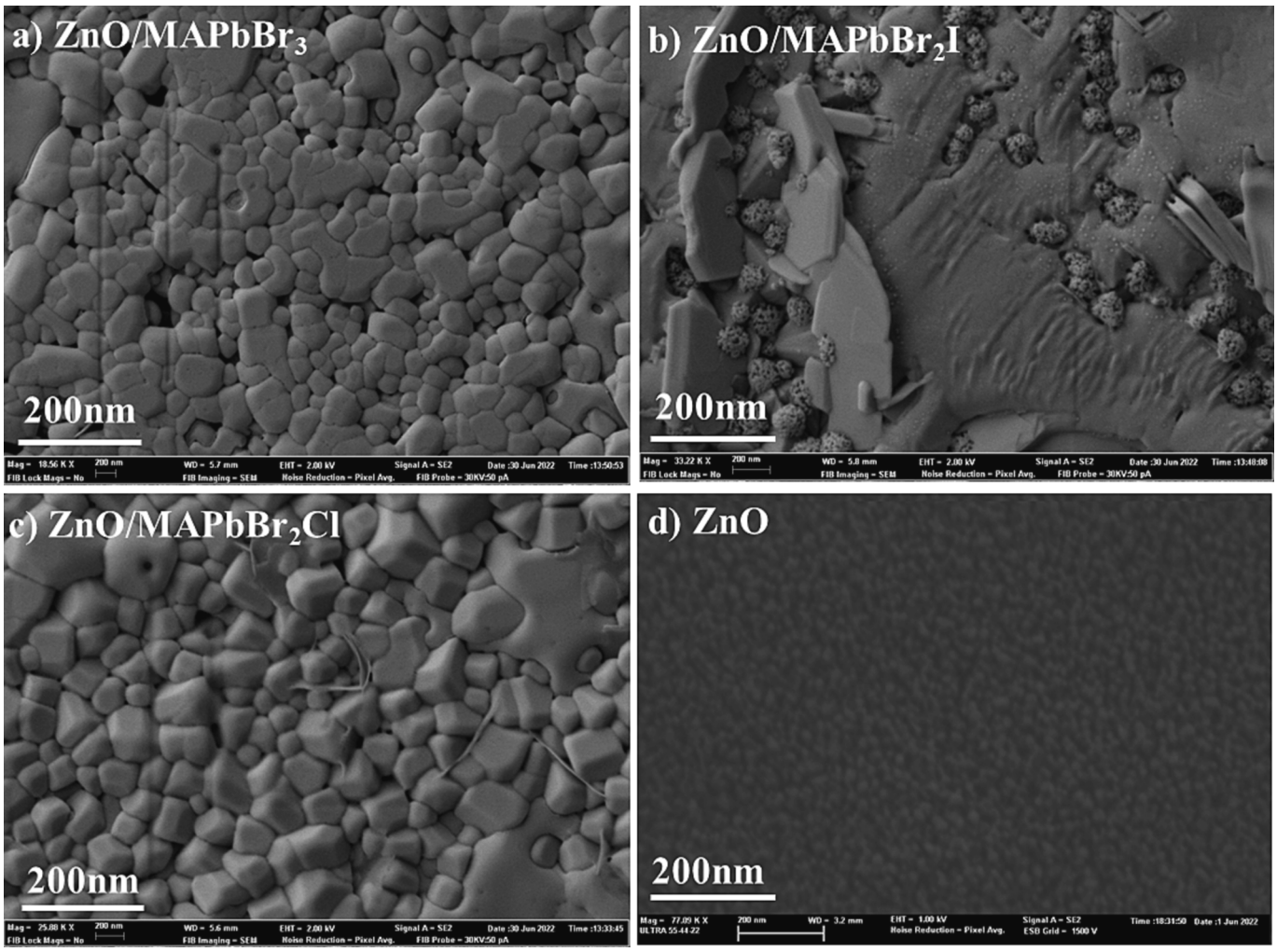

Fig. 4. SEM images of films: a) ZnO/$MAPbBr_3$; b) ZnO/$MAPbBr_2I$; c) ZnO/$MAPbBr_2Cl$; d) ZnO.

3. Results and discussions

3.1. XRD analysis

The perovskite samples ($MAPbBr_3$, $MAPbBr_2I$, and $MAPbBr_2Cl$) were examined by XRD to see the effect of halogen mixing on the structural properties of the different films produced. The ZnO layers without the perovskite were also examined by XRD. The results obtained are shown in Fig. 2 below. The results show that all samples exhibit two main peaks at $2\theta = 14.79°$ and $2\theta = 29.83°$ for the (1 0 0) and (2 0 0) crystallographic planes respectively. These two peaks indicate that the films produced are in a single phase. Our results agree with the literature (Jang et al., 2015; Doumbia et al., 2022). The intensity of the $MAPbBr_3$ peak increased when mixed with iodine (ZnO/$MAPbBr_2I$) and decreased when mixed with chlorine (ZnO/$MAPbBr_2Cl$). The ZnO film showed two main peaks located at $2\theta = 33.66°$ and $2\theta = 37.69°$. These peaks correspond to the (0 0 2) and (1 0 1) planes of the hexagonal wurtzite structure of ZnO respectively (JCPDS Card N° 00–036-1451). These ZnO films produced are polycrystalline.

Fig. 2b shows the maximum width at half maximum (FWHM) curves of the heterojunction films produced for the (1 0 0) and (2 0 0) crystal planes.

The lattice deformation was calculated to gain insight into the grain defects and deformation of the produced samples. Equation (1) below was used to determine the effective lattice strain (Ullah et al., 2020; Ullah et al., 2020).

$$\beta\cos(\theta) = (\lambda k)/D + 4\varepsilon\sin(\theta) \quad (1)$$

where β: FWHM; k = 0.94; θ: Bragg angle; D: the grain size; ε: lattice strain, and λ = 0.1540 nm: the wavelength of the X-ray.

The dislocation density of the lattice was calculated using equation (2) (Bouich et al., 2019).

$$\delta = 1/D^2 \quad (2)$$

The different values of the calculated parameters are summarised in Table 1 below. The grain size was given by X-ray.

The grain sizes which are shown in Table 1 above range from 401 nm to 747 nm. The bromine-based sample ($MAPbBr_3$) has the largest grain size of 747 nm. This grain size decreases with the mixing of iodine and chlorine. The size decreases considerably with iodine mixing and slightly with chlorine mixing (Doumbia et al., 2022). The small size of $MAPbBr_2I$ grains compared with the other samples may be due to the fact that iodine and bromine do not combine easily to form large grains.

As for the lattice deformation of the films produced, the values vary from 0.159 to 0.350. The smallest value is that of the bromine-based sample without mixing and the largest value is that of the sample mixed with iodine. The mixing then deforms the network. This deformation is significant with iodine. Also, the bromine-based sample without mixing has the lowest dislocation density of the order of 1.79 ×

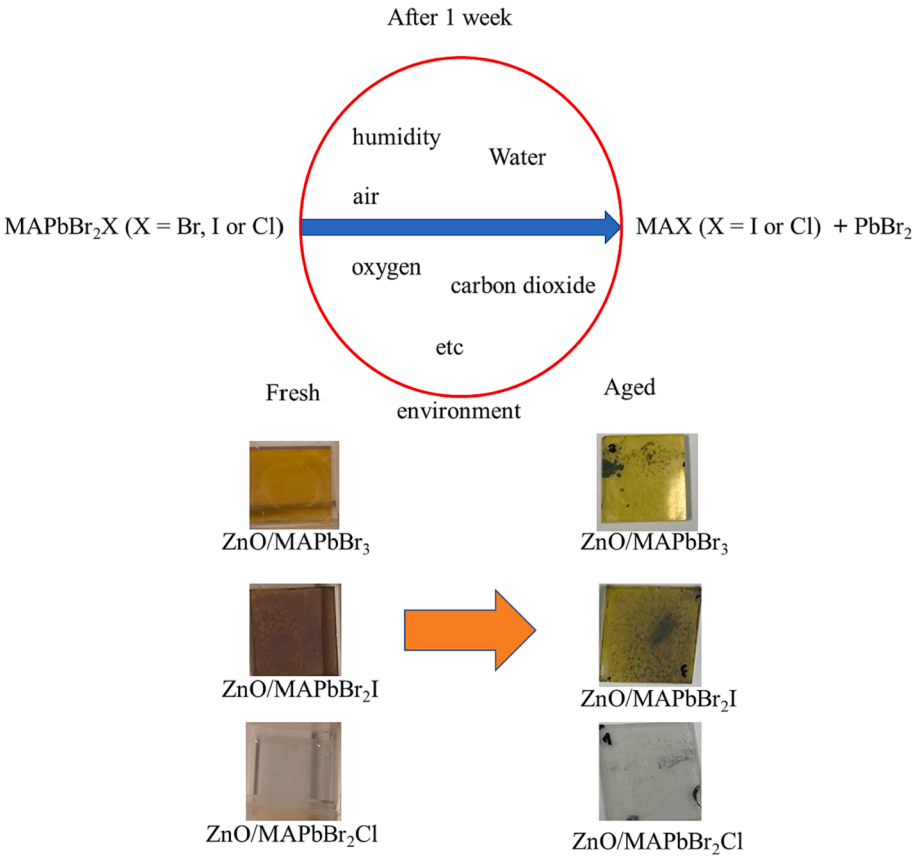

Fig. 5. Degradation Mechanism of perovskite films.

Table 2
Band gap of films.

Sample ID	ZnO	$ZnO/MAPbBr_3$	$ZnO/MAPbBr_2I$	$ZnO/MAPbBr_2Cl$
Band gap (eV)	3.28	2.4	2.15	2.25
Wavelength (nm)	543.8	516.6	576.5	551

10^{-6} nm^{-2}. This dislocation density increased with mixing and its largest value is that of the iodine-based sample.

3.2. Optical properties

The films produced were also characterized to determine their optical properties. Some of the optical properties such as absorbance and band gap are shown in Fig. 3 below. Fig. 3a shows the absorbance of the samples. This figure shows that the absorbance of the heterojunction films is much higher than that of the ZnO layer. The different perovskites deposited on the ZnO layer are all good absorbers. However, the curves show that the absorption of the sample increases when mixed with iodine and decreases when mixed with chlorine.

The band gaps of the samples are shown in Fig. 4b and 4c. The smallest band gap of the heterojunctions is 2.15 eV. This is the band gap of $ZnO/MAPbBr_2I$. Mixing has decreased the band gap of $ZnO/MAPbBr_3$. The band gap of the ZnO film on which the perovskite is deposited is 3.28 eV. This result corresponds to those found in the literature (Srikant and Clarke, 1998).Fig. 5..

The band gaps were calculated using the Tauc equation (Sharma et al., 2016; Koné et al., 2023; Koné et al., 2023).

$$(\alpha h\nu)^2 = \beta\,(h\nu - Eg) \quad (3)$$

With β a constant and α the absorption coefficient.

The band gap was determined by extrapolation by constructing the function $(\alpha h\nu)^2$ as a function of the energy hν (Bouich, 2021). We have summarised the results in Table 2 below.

3.3. SEM analysis

The surface morphology of the samples was studied. Fig. 4 below shows the SEM results of the films produced. We can notice in Fig. 4a, 4b, and 4c the presence of perovskite which has well covered the ZnO layer. These figures show perovskite surfaces filled with grains. These grains are very visible in the chlorine and bromine-based samples. These results are in good agreement with the X-ray analyses (Table 1). Fig. 4d shows the surface of the ZnO layer. We can see a good coverage of the substrate and a good grain size. The perovskite layer deposited on the ZnO creates an interface between the two layers through which the diffusion of electrons takes place. These electrons are generated in the perovskite layer when it receives solar radiation. This electron scattering causes surface defects in both layers.

3.4. Degradation study

Perovskite is a material that degrades quickly, especially in contact

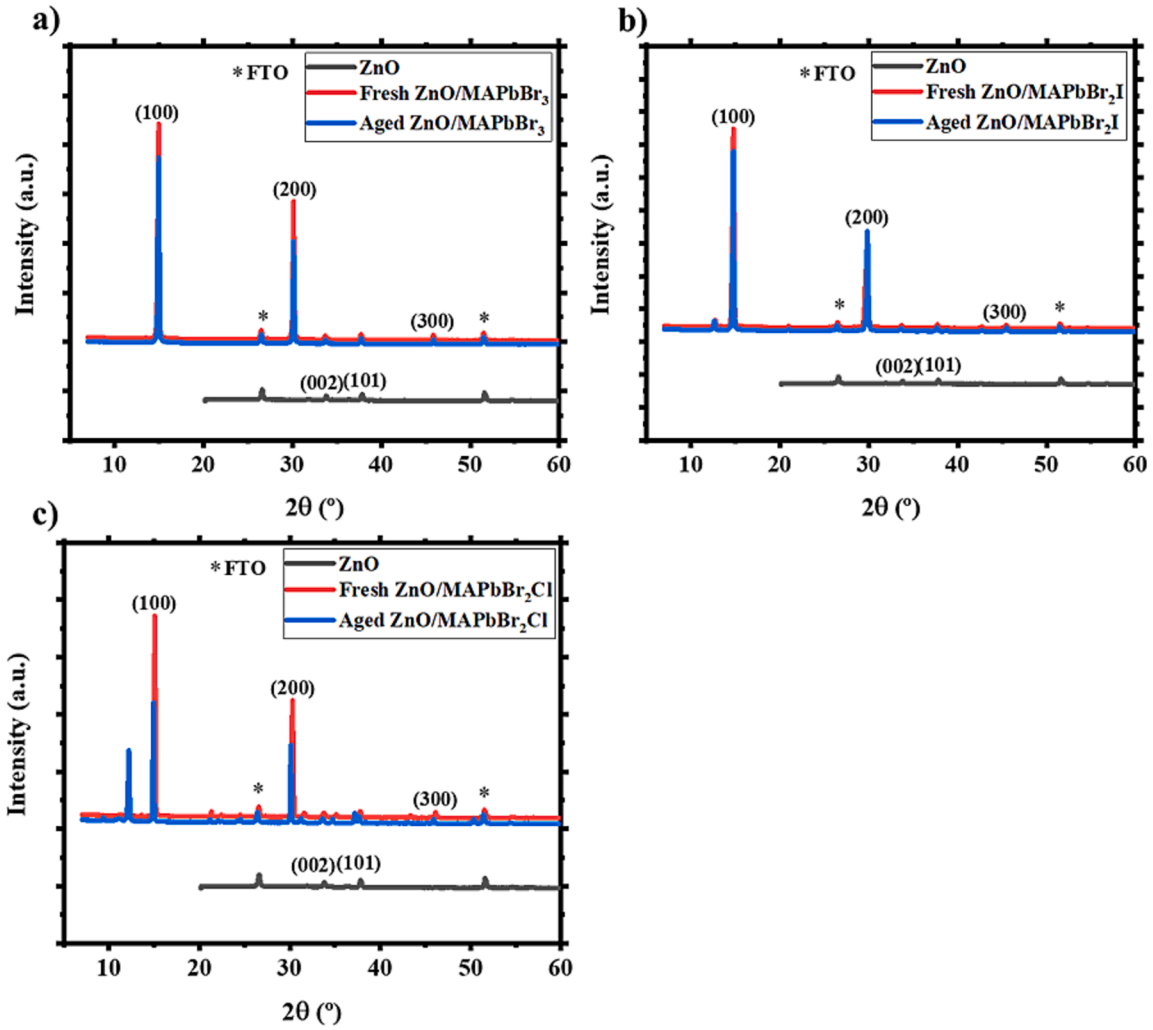

Fig. 6. XRD patterns of fresh and aged heterojunction films: a) $MAPbBr_3$, b) $MAPbBr_2I$, c) $MAPbBr_2Cl$.

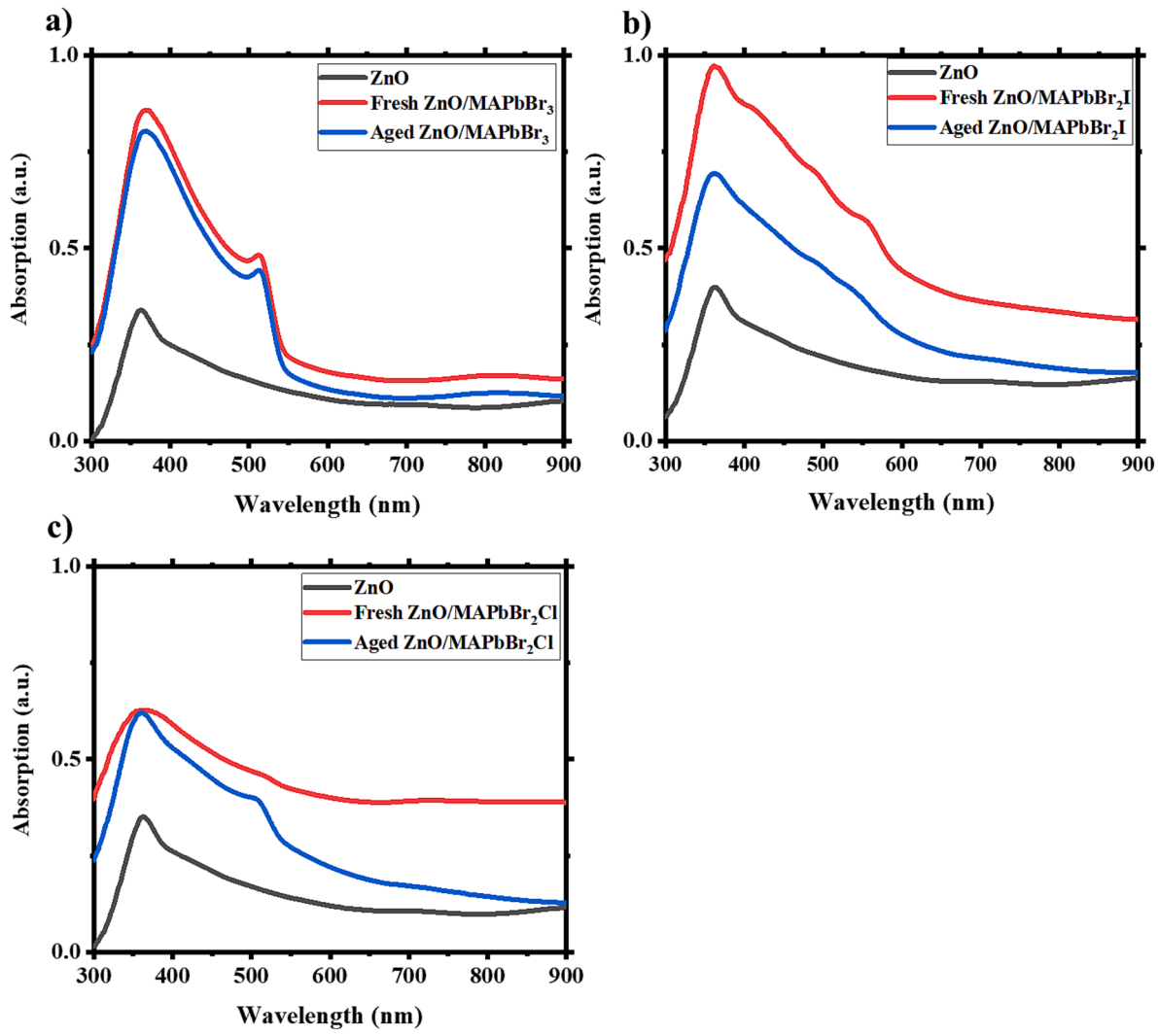

Fig. 7. Absorbance of fresh and aged heterojunction samples.

with humidity (Niu et al., 2015; Bouich et al., 2023). The degradation study was done one week after producing the films in this section, we want to see the effect of mixing on the degradation of the films. The degradation mechanism of perovskite is summarised in Fig. 6 below.

The degradation of the samples was studied by XRD, SEM, and UV–Visible analysis.

We can see the XRD patterns in Fig. 7 below. There is a decrease in peak intensity for each of the samples. This decrease in peak intensity is greater for the iodine sample. This XRD result thus shows that the iodine-based sample is less stable. We can see in the figure that the perovskite-based samples have undergone a degradation process while the ZnO-based sample has not degraded. ZnO is therefore a much more stable material.

Fig. 7 below shows the absorption of fresh and aged films. For each sample, the absorption decreased one week later. We can see in Fig. 7b that this decrease is very important for the iodine-based sample. One week later, the iodine-based sample degraded the most. Its absorption has decreased considerably. In this case, it is the least stable.

We have illustrated the SEM surface morphology of the aged films in Fig. 8 below. Each of the surfaces of the films is degraded. There are surface defects and holes. We record holes on the surface of the ZnO/$MAPbBr_3$ and ZnO/$MAPbBr_2Cl$ films. For the iodine-based sample, holes and surface defects are observed.

4. Conclusion

At the end of this work, it is found that mixing influences the different properties of the ZnO/$MAPbBr_3$ sample. XRD results showed that all perovskite samples have two main peaks at $2\theta = 14.79°$ and $2\theta = 29.83°$ for the (1 0 0) and (2 0 0) crystallographic planes respectively. These results also showed that the crystallinity decreased with mixing. The ZnO/$MAPbBr_3$ sample without mixing is the one with the best crystallinity. Next comes the sample mixed with chlorine. XRD analysis of the ZnO films showed two main peaks located at $2\theta = 33.66°$ and $2\theta = 37.69°$ which correspond to the (0 0 2) and (1 0 1) planes of the hexagonal wurtzite structure of ZnO respectively. These ZnO films produced are polycrystalline. The SEM images show good coverage of the perovskite on the ZnO layer. The grains are noticeable for all samples. But the ZnO/MAPbBr3 sample shows the best crystallinity. The UV–Visible analysis showed that the sample mixed with iodine absorbs the most and therefore has the smallest band gap of 2.15 eV. The band gaps of the heterojunction samples range from 2.15 eV to 2.40 eV. That of the ZnO layer is 3.28 eV. These different samples degrade in contact with air and humidity. However, the sample mixed with iodine degrades more rapidly.

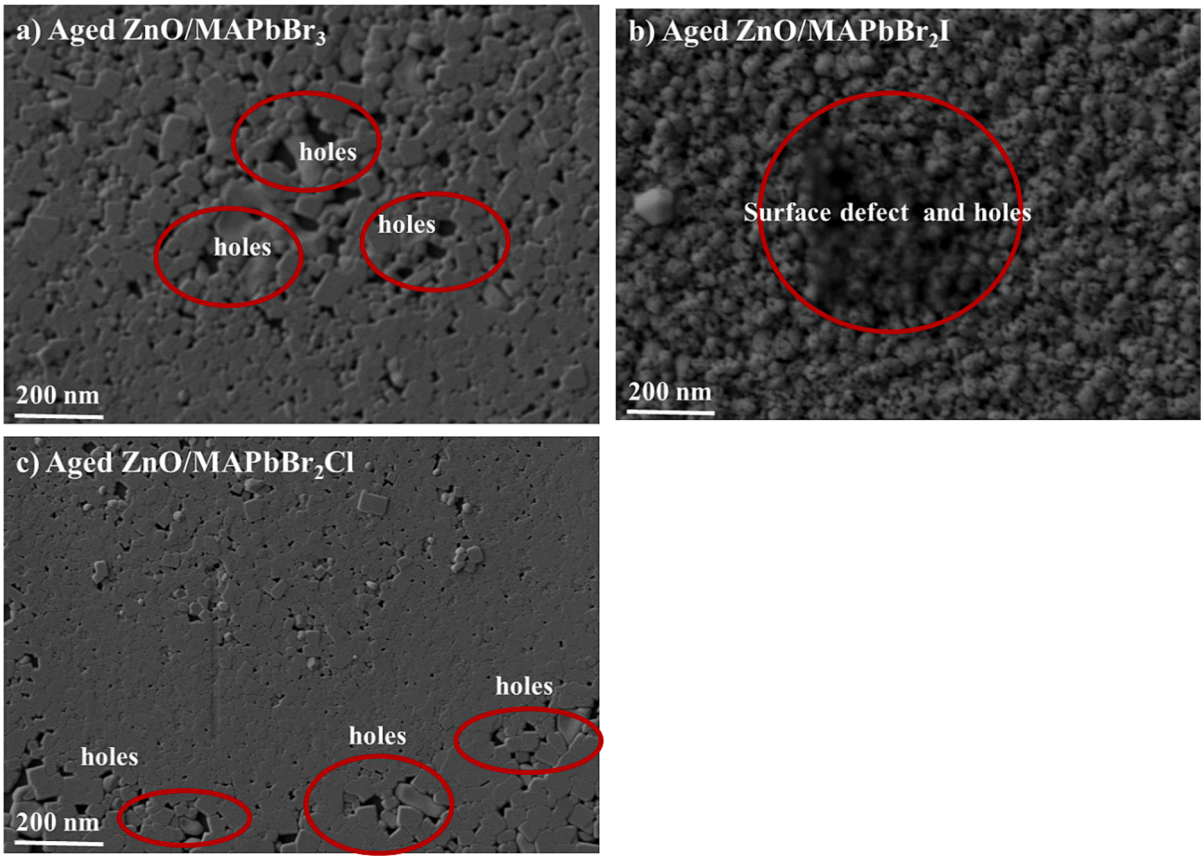

Fig. 8. SEM image of aged samples: a) $ZnO/MAPbBr_3$, b) $ZnO/MAPbBr_2I$, c) $ZnO/MAPbBr_2Cl$.

Declaration of Competing Interest

The authors declare that they have no known competing financial interests or personal relationships that could have appeared to influence the work reported in this paper.

Data availability

all data included in the manuscript

Acknowledgments

Author Klègayéré Emmanuel Koné thanks Erasmus + KA107 for the grant.

Amal Bouich acknowledges Ministerio de Ciencia e Innovación (Spain) for funding support through Margarita Salas Fellowship (MCIN/AEI/10.13039/501100011033). This work has been funded by the Conselleria d'Innovació, Universitats, Ciència i Societat Digital (Generalitat valenciana, Prometeus 2023 CIPROM2022/03) and the Agencia Estatal de Investigación (Spain) through project PID2019-107137RB-C21/AEI/10.13039/501100011033 and by ERDF under the funding "A way of making Europe". (Bouazizi et al., 2022).

References

Bouazizi, S., Tlili, W., Bouich, A., Soucase, B.M., Omri, A., 2022. Design and efficiency enhancement of FTO/PC60BM/CsSn0. 5Ge0. 5I3/Spiro-OMeTAD/Au perovskite solar cell utilizing SCAPS-1D Simulator. Materials Research Express 9 (9), 096402.

Bouich, A., Hartiti, B., Ullah, S., Ullah, H., Ebn Touhami, M., Santos, D.M.F., Mari, B., 2019. Optoelectronic characterization of CuInGa (S) 2 thin films grown by spray pyrolysis for photovoltaic application. Appl. Phys. A 125, 1–9.

Bouich, A. (2021). *Study and characterization of hybrid perovskites and copper-indium-gallium selenide thin films for tandem solar cells* (Doctoral dissertation, Universitat Politècnica de València).https://doi.org/10.4995/Thesis/10251/160621.

Bouich, A., Marí-Guaita, J., Bouich, A., Pradas, I.G., Marí, B., 2022. Towards manufacture stable lead perovskite APbI3 (A= Cs, MA, FA) based solar cells with low-cost techniques. Engineering Proceedings 12 (1), 81.

Bouich, A., Marí-Guaita, J., Soucase, B.M., Palacios, P., 2023. Bright future by enhancing the stability of methylammonium lead triiodide perovskites thin films through Rb, Cs and Li as dopants. Mater. Res. Bull. 163, 112213.

Bouich, A., Torres, J.C., Chfii, H., Marí-Guaita, J., Khattak, Y.H., Baig, F., Soucase, B.M., Palacios, P., 2023. Delafossite as hole transport layer a new pathway for efficient perovskite-based solar sells: Insight from experimental, DFT and numerical analysis. Sol. Energy 250, 18–32.

Bouich, A., Torres, J.C., Khattak, Y.H., Baig, F., Marí-Guaita, J., Soucase, B.M., Mendez-Blas, A., Palacios, P., 2023. Bright future by controlling α/δ phase junction of formamidinium lead iodide doped by imidazolium for solar cells: insight from experimental, DFT calculations and SCAPS simulation. Surf. Interfaces 40, 103159.

Bouri, N., Talbi, A., Khaaissa, Y., Derbali, S., Bouich, A., Nouneh, K., 2022. Insight into MAPb1− xEuxI3 based perovskite solar cell performance using SCAPS Simulator. Optik 271, 170235.

Burschka, J., Pellet, N., Moon, S.J., Humphry-Baker, R., Gao, P., Nazeeruddin, M.K., Grätzel, M., 2013. Sequential deposition as a route to high-performance perovskite-sensitized solar cells. Nature 499 (7458), 316–319.

Chang, C. Y., Tsao, F. C., Pan, C. J., Chi, G. C., Wang, H. T., Chen, J. J., ... & Chen, L. C. (2006). Electroluminescence from ZnO nanowire/polymer composite p-n junction. Applied Physics Letters, 88(17), 173503.

De Wolf, S., Holovsky, J., Moon, S.-J., Löper, P., Niesen, B., Ledinsky, M., Haug, F.-J., Yum, J.-H., Ballif, C., 2014. Organometallic halide perovskites: sharp optical absorption edge and its relation to photovoltaic performance. The Journal of Physical Chemistry Letters 5 (6), 1035–1039.

Doumbia, Y., Bouich, A., Soro, D., Soucase, B.M., 2022. Mixed halide head perovskites thin films: Stability and growth investigation. Optik 261, 169222.

Fakharuddin, A., Shabbir, U., Qiu, W., Iqbal, T., Sultan, M., Heremans, P., et al., 2019. Inorganic and layered perovskites for optoelectronic devices. Adv. Mater. 31 (47), 1807095. https://doi.org/10.1002/adma.201807095.

Gledhill, S., Grimm, A., Allsop, N., Koehler, T., Camus, C., Lux-Steiner, M., Fischer, C.H., 2009. A spray pyrolysis route to the undoped ZnO layer of Cu (In, Ga)(S, Se) 2 solar cells. Thin Solid Films 517 (7), 2309–2311.

Gu, X., Li, C., Yuan, S., Ma, M., Qiang, Y., Zhu, J., 2016. ZnO based heterojunctions and their application in environmental photocatalysis. Nanotechnology 27 (40), 402001.

Hwang, S.H., Chung, T.H., Lee, B.T., 2009. Study on the interfacial layer in ZnO/GaN heterostructure light-emitting diode. Mater. Sci. Eng. B 157 (1–3), 32–35.

Im, J.H., Lee, C.R., Lee, J.W., Park, S.W., Park, N.G., 2011. 6.5% efficient perovskite quantum-dot-sensitized solar cell. Nanoscale 3 (10), 4088–4093.

Jang, D.M., Park, K., Kim, D.H., Park, J., Shojaei, F., Kang, H.S., Ahn, J.-P., Lee, J.W., Song, J.K., 2015. Reversible halide exchange reaction of organometal trihalide perovskite colloidal nanocrystals for full-range band gap tuning. Nano Lett. 15 (8), 5191–5199.

Jeon, N.J., Noh, J.H., Yang, W.S., Kim, Y.C., Ryu, S., Seo, J., Seok, S.I., 2015. Compositional engineering of perovskite materials for high-performance solar cells. Nature 517 (7535), 476–480.

Kojima, A., Teshima, K., Shirai, Y., Miyasaka, T., 2009. Organometal halide perovskites as visible-light sensitizers for photovoltaic cells. J. Am. Chem. Soc. 131 (17), 6050–6051.

Koné, K.E., Bouich, A., Soro, D., Soucase, B.M., 2023. Surface engineering of zinc oxide thin as an electron transport layer for perovskite solar cells. Opt. Quant. Electron. 55 (7), 1–11.

Koné, K.E., Bouich, A., Soucase, B.M., Soro, D., 2023. Manufacture of different oxides with high uniformity for copper zinc tin sulfide (CZTS) based solar cells. J. Mol. Graph. Model. 121, 108448.

Koné, K.E., Bouich, A., Marí-Guaita, J., Soucase, B.M., Soro, D., 2023. Insight into the effect of halogen X in methylammonium lead halide (MAPbX3) spin-coated on zinc oxide film. Opt. Mater. 135, 113238.

Lee, M.M., Teuscher, J., Miyasaka, T., Murakami, T.N., Snaith, H.J., 2012. Efficient hybrid solar cells based on meso-superstructured organometal halide perovskites. Science 338 (6107), 643–647.

Leijtens, T., Stranks, S.D., Eperon, G.E., Lindblad, R., Johansson, E.M.J., McPherson, I.J., Rensmo, H., Ball, J.M., Lee, M.M., Snaith, H.J., 2014. Electronic properties of meso-superstructured and planar organometal halide perovskite films: charge trapping, photodoping, and carrier mobility. ACS Nano 8 (7), 7147–7155.

Leijtens, T., Eperon, G.E., Noel, N.K., Habisreutinger, S.N., Petrozza, A., Snaith, H.J., 2015. Stability of metal halide perovskite solar cells. Adv. Energy Mater. 5 (20), 1500963.

Lin, Q., Armin, A., Nagiri, R.C.R., Burn, P.L., Meredith, P., 2015. Electro-optics of perovskite solar cells. Nat. Photonics 9 (2), 106–112.

Look, D.C., Coşkun, C., Claflin, B., Farlow, G.C., 2003. Electrical and optical properties of defects and impurities in ZnO. Phys. B Condens. Matter 340, 32–38.

Masuko, K., Shigematsu, M., Hashiguchi, T., Fujishima, D., Kai, M., Yoshimura, N., Yamaguchi, T., Ichihashi, Y., Mishima, T., Matsubara, N., Yamanishi, T., Takahama, T., Taguchi, M., Maruyama, E., Okamoto, S., 2014. Achievement of more than 25% conversion efficiency with crystalline silicon heterojunction solar cell. IEEE J. Photovoltaics 4 (6), 1433–1435.

N'guessan, A.I., Bouich, A., Touré, A., Soucasse, B.M., Soro, D., 2023. Influence of sulfur content in Zn (O, S) buffer layer onto copper indium gallium sulfur-based solar cells through surface engineering at ZnO1− x S x/CIGS interface. JOM 75 (10), 4332–4340.

Niu, G., Guo, X., Wang, L., 2015. Review of recent progress in chemical stability of perovskite solar cells. J. Mater. Chem. A 3 (17), 8970–8980.

Oyedele, S., Boko, A.K.A., Marí, B., 2017. Optimisation des paramètres photovoltaïques du CIGS al aide du simulateur AMPS-1D. Afrique Science 13 (2), 274–283.

Schmidt, T.M., Larsen-Olsen, T.T., Carlé, J.E., Angmo, D., Krebs, F.C., 2015. Upscaling of perovskite solar cells: fully ambient roll processing of flexible perovskite solar cells with printed back electrodes. Adv. Energy Mater. 5 (15), 1500569.

Shao, D., Zhu, W., Xin, G., Liu, X., Wang, T., Shi, S., Lian, J., Sawyer, S., 2020. A high performance UV–visible dual-band photodetector based on an inorganic Cs 2 SnI 6 perovskite/ZnO heterojunction structure. J. Mater. Chem. C 8 (5), 1819–1825.

Sharma, R., Acharya, A.D., Shrivastava, S.B., Patidar, M.M., Gangrade, M., Shripathi, T., Ganesan, V., 2016. Studies on the structure optical and electrical properties of Zn-doped NiO thin films grown by spray pyrolysis. Optik 127 (11), 4661–4668.

Srikant, V., & Clarke, D. R. (1998). On the optical band gap of zinc oxide. Journal of Applied Physics, 83(10), 5447-5451.

Stranks, S.D., Eperon, G.E., Grancini, G., Menelaou, C., Alcocer, M.J., Leijtens, T., Snaith, H.J., 2013. Electron-hole diffusion lengths exceeding 1 micrometer in an organometal trihalide perovskite absorber. Science 342 (6156), 341–344.

Tang, M.-C., Dang, H.X., Lee, S., Barrit, D., Munir, R., Wang, K., Li, R., Smilgies, D.-M., De Wolf, S., Kim, D.-Y., Anthopoulos, T.D., Amassian, A., 2021. Wide and tunable bandgap MAPbBr 3− xClx hybrid perovskites with enhanced phase stability: in situ investigation and photovoltaic devices. Solar RRL 5 (4).

Touré, A., Bouich, A., Doumbia, Y., Soucasse, B.M., Soro, D., 2023. Investigation of the optoelectronic and structural properties of FA (1–x) BixPbBr 6I3 of perovskite mixed halide films. Optik 288, 171160.

Ullah, S., Bouich, A., Ullah, H., Mari, B., Mollar, M., 2020. Enhanced optical and structural properties of V-doped binary SnS2 buffer layer. Sol. Energy 204, 654–659.

Ullah, S., Bouich, A., Ullah, H., Mari, B., Mollar, M., 2020. Comparative study of binary cadmium sulfide (CdS) and tin disulfide (SnS2) thin buffer layers. Sol. Energy 208, 637–642.

Weidman, M. C., Seitz, M., and Tisdale, W. A. (2019). U.S. Patent No. 10,273,405 (Washington, DC: U.S. Patent and Trademark Office).

Xing, G., Mathews, N., Sun, S., Lim, S.S., Lam, Y.M., Grätzel, M., Sum, T.C., 2013. Long-range balanced electron-and hole-transport lengths in organic-inorganic CH3NH3PbI3. Science 342 (6156), 344–347.

Zhao, D., Sexton, M., Park, H.Y., Baure, G., Nino, J.C., So, F., 2015. High-efficiency solution-processed planar perovskite solar cells with a polymer hole transport layer. Adv. Energy Mater. 5 (6), 1401855.

Zhou, H., Chen, Q., Li, G., Luo, S., Song, T.B., Duan, H.S., Yang, Y., 2014. Interface engineering of highly efficient perovskite solar cells. Science 345 (6196), 542–546.